American Mineralogist, Volume 105, pages 455–467, 2020

Micro- and nano-size hydrogarnet clusters and proton ordering in calcium silicate garnet: Part I. The quest to understand the nature of "water" in garnet continues

Charles A. Geiger[1,*,†] and George R. Rossman[2]

[1]Department of Chemistry and Physics of Materials, Section Materials Science and Mineralogy, Salzburg University, Jakob Haringer Strasse 2a, A-5020 Salzburg, Austria

[2]Division of Geological and Planetary Sciences, California Institute of Technology, Pasadena, California 91125-2500, U.S.A.

Abstract

The calcium-silicate garnets, grossular ($Ca_3Al_2Si_3O_{12}$), andradite ($Ca_3Fe^{3+}_2Si_3O_{12}$), and their solid solutions [$Ca_3(Al_x,Fe^{3+}_{1-x})_2Si_3O_{12}$], can incorporate various amounts of structural OH^-. This has important mineralogical, petrological, rheological, and geochemical consequences and extensive experimental investigations have focused on the nature of "water" in these phases. However, it was not fully understood how OH^- was incorporated and this has seriously hampered the interpretation of different research results. IR single-crystal spectra of several nominally anhydrous calcium silicate garnets, both "end-member" and solid-solution compositions, were recorded at room temperature and 80 K between 3000 and 4000 cm^{-1}. Five synthetic hydrogarnets in the system $Ca_3Al_2(SiO_4)_3$-$Ca_3Al_2(H_4O_4)_3$-$Ca_3Fe^{3+}_2(SiO_4)_3$-$Ca_3Fe^{3+}_2(H_4O_4)_3$ were also measured via IR ATR powder methods. The various spectra are rich in complexity and show several OH^- stretching modes at wavenumbers between 3500 and 3700 cm^{-1}. The data, together with published results, were analyzed and modes assigned by introducing atomic-vibrational and crystal-chemical models to explain the energy of the OH^- dipole and the structural incorporation mechanism of OH^-, respectively. It is argued that OH^- is located in various local microscopic- and nano-size $Ca_3Al_2H_{12}O_{12}$- and $Ca_3Fe^{3+}_2H_{12}O_{12}$-like clusters. The basic substitution mechanism is the hydrogarnet one, where $(H_4O_4)^{4-} \leftrightarrow (SiO_4)^{4-}$, and various local configurations containing different numbers of $(H_4O_4)^{4-}$ groups define the cluster type. Some spectra also possibly indicate the presence of tiny hydrous inclusion phases, as revealed by OH^- modes above about 3670 cm^{-1}. They were not recognized in earlier studies. Published proposals invoking different hypothetical "defects" and coupled-substitution mechanisms involving H^+ are not needed to interpret the IR spectra, at least for OH^- modes above about 3560 cm^{-1}. Significant mineralogical, petrological, and geochemical consequences result from the analysis and are discussed in the accompanying Part II (this issue) of the investigation.

Keywords: Grossular, andradite, nominally anhydrous minerals, H_2O, hydrogarnet clusters, nanoscale, IR spectroscopy; Water in Nominally Hydrous and Anhydrous Minerals

Introduction

Garnet is a remarkable phase for several reasons (Geiger 2013). One of them is its ability to adapt its crystal structure to accommodate radically different compositions. Indeed, garnet, as both a synthetic phase and as a mineral, exhibits vast chemical variability. One interesting system is the loosely termed "hydrogarnets" or "water"-bearing garnets. The general crystal-chemical formula of anhydrous or "water-free" garnet is $\{X_3\}[Y_2](Z_3)O_{12}$, where dodecahedral $\{X\}$, octahedral $[Y]$, and tetrahedral (Z) represent the three special crystallographic cation sites and their polyhedral coordination in space group $Ia\bar{3}d$. In most rock-forming garnets, $Z = Si^{4+}$. In true "hydrogarnet," however, the crystallographically single Z cation is absent and, instead, it is replaced and charge balanced locally by four protons. The resulting general crystal-chemical formula can be written as $\{X_3\}[Y_2](H_{12})O_{12}$ or $\{X_3\}[Y_2](H_4O_4)_3$. The former expression is more suitable for describing the vibrational behavior of hydrogarnet and the latter the static crystal chemistry (see discussion below).

Cornu (1905, 1906) was the first to discover hydrogarnet, which he termed hibschite. Other reports of hydrogarnet followed (e.g., Foshag 1920; Belyankin and Petrov 1939; Belyankin and Petrov 1941a) and Foshag introduced the name plazolite for his specimen. Belyankin and Petrov (1941a, 1941b), in their studies, offered the first simplified and correct formula for hibschite as $3CaO{\cdot}Al_2O_3{\cdot}2SiO_2{\cdot}2H_2O$. Passaglia and Rinaldi (1984) analyzed the situation and proposed that the term katoite should be reserved for $Ca_3Al_2(SiO_4)_3$-$Ca_3Al_2(H_4O_4)_3$ garnets with more than 50 mol% of the latter component and hibschite for those with less than 50%. These two workers, as well as Ferro et al. (2003), described new katoite localities and investigated the garnet crystal structures.

It may well have been that Thorvaldson and Grace (1929) and Thorvaldson et al. (1929) were the first to synthesize and characterize $Ca_3Al_2(H_4O_4)_3$. It can be easily synthesized by reacting $Ca_3Al_2O_6$ with water at 1 atm. The reaction is highly exothermic, and it is important in the crystallization sequence of some cements including portlandite. Flint et al. (1941) showed that there can be complete solid solution between $Ca_3Al_2(H_4O_4)_3$ and $Ca_3Al_2(SiO_4)_3$

* E-mail: ca.geiger@sbg.ac.at

† Special collection papers can be found online at http://www.minsocam.org/MSA/AmMin/special-collections.html.

(see also Flint and Wells 1941; Carlson 1956; Kobayashi and Shoji 1983; Dilnesa et al. 2014). The exchange $(H_4O_4)^{4-} \leftrightarrow (SiO_4)^{4-}$ or $4(H)^+ \leftrightarrow (Si)^{4+}$ was, thus, indicated. Crystal structure determinations of synthetic $Ca_3Al_2(H_4O_4)_3$ using diffraction experiments proved this (Cohen-Addad et al. 1967; Foreman 1968; Lager et al. 1987). Such complete exchange between four protons and a single Si^+ cation in a silicate is unique in the mineralogical kingdom, as best we know. More recent synthesis results have shown that the degree of solid solution is temperature dependent and that a miscibility gap can exist along the $Ca_3Al_2(H_4O_4)_3$-$Ca_3Al_2(SiO_4)_3$ join (Jappy and Glasser 1991). Water-rich hydrogrossular occurs in relatively low-temperature geologic environments consistent with its *P-T* phase stability (Flint et al. 1941; Carlson 1956; Dilnesa et al. 2014). Yoder (1950) investigated the high *P-T* phase relations of grossular under dry and hydrothermal conditions and discussed the stability of $Ca_3Al_2(SiO_4)_3$-$Ca_3Al_2(H_4O_4)_3$ solid solutions. His study was extended by Pistorius and Kennedy (1960) in their experimental high *P-T* investigation of grossular and hydrogrossular.

Other hydrogarnets, both end-member and solid-solution compositions, have been prepared in the laboratory (e.g., Ito and Frondel 1967; Li et al. 1997; Albrecht et al. 2019), but none of them have been found in nature. The binary andradite $[Ca_3Al_2(SiO_4)_3]$-"hydroandradite" $[Ca_3Al_2(H_4O_4)_3]$ has been demonstrated by laboratory synthesis experiments to show an extensive degree of substitutional solid solution (Flint et al. 1941; Dilnesa et al. 2014). The precise phase relations are difficult to determine because of kinetic issues. The synthesis of end-member $Ca_3Fe_2^{3+}(H_4O_4)_3$ has apparently not yet been fully achieved (e.g., Kuzel 1968), and its thermodynamic stability appears to be restricted to below roughly 60 °C (Lothenbach, personal communication). Kresten et al. (1982) reported the occurrence of a hydroandradite from Sweden, and Armbruster (1995) refined the crystal structure a hydrous andradite from South Africa.

"Water" in nominally anhydrous silicate garnet

An initial report (Wilkins and Sabine 1973) of various rock-forming silicates containing small concentrations of H_2O, including garnet, was largely ignored for years and probably was viewed as a "mineralogical curiosity" by the broader community. However, following reports of the presence of OH^- in different rock-forming garnet species (e.g., Beran et al. 1983; Aines and Rossman 1984), which, moreover, could be measured straightforwardly with IR single-crystal methods, research in this area intensified. Study has been also directed at a number of other so-called "NAMs," which is short for nominally anhydrous minerals. Interest increased greatly and scientists began discussing, for example, how many "oceans of water" could be contained in Earth's upper mantle (Bell and Rossman 1992) and the geochemical and geophysical ramifications. Important mineral groups like olivine, pyroxene, and feldspar, for example, were studied in various ways and in terms of their minor water contents (see reviews of Ingrin and Skogby 2000 and Peslier 2010). The state of research on NAMs is now mature.

To determine the presence of OH^- in garnet, or any other nominally anhydrous mineral for that matter, IR spectroscopy has been the method of choice. Legions of IR single-crystal spectra (and some Raman spectra as well) have been recorded on various garnet species and compositions, both natural and synthetic. They show a plethora of different energy vibrational OH^- stretching modes. However, in spite of the great amount of study, conclusive assignments of the protons to exact structural sites in the crystals have remained elusive. The nature of these minor concentration OH^- groups in garnet is not well understood in a crystal-chemical sense, with a few exceptions (see Geiger and Rossman 2018). It is not understood if the OH^- groups are just some ill-defined defect(s) or whether they occupy more than one crystallographic position in an ordered manner (e.g., Birkett and Trzcienski 1984; Basso et al. 1984; Basso and Cabella 1990). Or does their presence represent some atomic-coupled-substitution mechanism, for example, $(Al^{3+}\text{-}H^+)^{4+} = (Si^{4+})$ or are they linked to "nonstandard garnet" elements, such as $\{Li^+\text{-}H^+\} = \{Ca,Mg,Fe^{2+},Mn^{2+}\}$ [see references and discussion in Part II (Geiger and Rossman 2020b)]? Most astonishingly, considering the degree of study and the "stage of the game," it is not known how structural OH^- is incorporated in most natural garnets [e.g., as $(H_4O_4)^{4-}$ groups or not]. Proton NMR study of synthetic katoite and three natural grossulars showed, depending on the exact garnet in question, the presence of four H-atom clusters (hydrogarnet) and/or two H-atom clusters (Cho and Rossman 1993).

Present thinking or the "ruling scientific mindset" considers that, because the IR spectra of nearly all natural silicate garnets do not match the IR spectra of their synthetic analogues, both in terms of the number of OH^- modes as well as their energies, the two types of crystals must have different OH^- substitutional mechanisms. With regard to the common silicate garnets, a match in IR spectra has only been found between synthetic and natural andradite (Geiger and Rossman 2018). However, the "ruling scientific mindset" that has operated over, say, the past three decades may be wrong. Radical new insight is needed to move beyond what has been observed, analyzed, and proposed over the last three decades in terms of OH^- in garnet.

Both this investigation and that in Part II (Geiger and Rossman 2020b) attempt to do this. The long quest to understand the nature of "water" in garnet, and researching the possible occurrence of the hydrogarnet substitution in natural garnets, continues. To do this, we studied OH^- substitution in the four component system $Ca_3Al_2(SiO_4)_3$-$Ca_3Al_2(H_4O_4)_3$-$Ca_3Fe_2^{3+}(SiO_4)_3$-$Ca_3Fe_2^{3+}(H_4O_4)_3$ by examining both synthetic and natural garnets. The main experimental input is from IR spectroscopy. An analysis of the results is undertaken that is based on the atomic-vibrational and crystal-chemical properties of calcium silicate garnets.

Samples used for study and experimental methods

The garnets measured via IR single-crystal and powder ATR spectroscopy are from the personal collections of CAG and GRR. The various samples are described in Table 1. Many of the single crystals have been characterized via microprobe analysis and studied in some form before, including by IR spectroscopy in the energy range between 3000 and 4000 cm^{-1}. For example, the large collection of grossular spectra of Rossman and Aines (1991) were measured with a grating spectrometer, whereas other spectra shown herein were measured with various Fourier-transform IR spectrometers. Newer and better spectrometers allow more spectral detail to be revealed. Moreover, several garnet crystals were measured at low temperatures, ultimately down to 80 K. The experimental setup in terms of the more recent measurements has been described before (e.g., Geiger and Rossman 2018).

TABLE 1. Description of natural and synthetic grossular, andradite, grossular-andradite, and hydrogarnet samples measured or used in this study

Garnet type & sample label	Type/locality (Source)	Sample description (*P-T*, color, thickness, reference)	Approximate garnet composition
Grossular	Synthetic grossular (C.A. Geiger)	T = 800 °C and P_{H_2O} = 0.2 GPa; 0.038 mm; Geiger and Armbruster (1997)	Gross100
Gr83	Synthetic grossular	T = 1000 °C and P_{H_2O} = 3.0 GPa; Digitalized data from Fig. 1 in Withers et al. (1998) normalized to 1 mm thickness	Gross100
Grossular GRR 53	Asbestos, Quebec, Canada (Shale's Lapidary)	Pale orange, "Hessonite", 0.139 mm; Rossman and Aines (1991)	Gross94Andr06
Grossular GRR 1038	Jeffrey Mine, Asbestos, Quebec, Canada (Rock H. Currier, Jewel Tunnel Imports)	Colorless rim, green colored core (Cr^{3+}), 0.276 mm; Rossman and Aines (1991)	Gross96Andr04
Grossular GRR 1042	Vesper Peak, Snohomish Co., WA, U.S.A. (Caltech collection, CIT-8197)	Orange-brown, 1.156 mm; Rossman and Aines (1991)	Gross86Andr14
Grossular GRR 1058	Synthetic hydrogrossular (G. Lager)	Synthetic (GL IV 2Sia), KBr pellet; Lager et al. (1987); Rossman and Aines (1991)	$Ca_3Al_2(O_4H_4)_3$
Grossular GRR 1059	Synthetic hydrogrossular (G. Lager)	Synthetic (GL VII 1), KBr pellet; Lager et al. (1987); Rossman and Aines (1991)	$Ca_3Al_2(SiO_4)_{2.28}(O_4H_4)_{0.72}$
Grossular GRR 1285	Jeffrey Mine, Asbestos, Quebec, Canada (F. Allen)	0.030 mm; light orangish pink; Cho and Rossman (1993); Allen and Buseck (1988)	Gross98Andr02
Grossular GRR 1329	Commercial Quarry, Crestmore, CA, U.S.A. (Pomona College, R.A. Crippen, RAC U-29)	Near-colorless "plazolite". Braided veins between gehlenite, ~12 um thick; Woodford et al. (1941); Rossman and Aines (1991)	–
Grossular GRR 1358	Commercial Quarry Crestmore, CA, U.S.A. (R. Basso - orginally from A. Pabst)	Colorless "Plazolite", 0.024 mm thick; Pabst (1942); Rossman and Aines (1991)	$Ca_3Al_2(SiO_4)_{1.82}(O_4H_4)_{1.18}$
Grossular 1386	Merelani Hills, Lelatema Mountains, Umba Valley, Aursha Region, Tanzania (Peter Flusser, Overland Gems, Los Angeles)	Nearly colorless, ~5 mm gemmy, water-worn, crystal fragment; Cho and Rossman (1993); Palke et al. (2015)	Gross99Andr01
Grossular 1420	Rauris Valley, Salzburger-Land, Austria (Caltech collection CIT-12534)	Orange crystals, 0.186 mm thick; Rossman and Aines (1991)	Gross75Andr25
Grossular 1424	Garnet Queen Mine (?), Santa Rosa Mountains, San Diego County, CA, U.S.A. (Caltech collection, CIT-8804)	Orange crystals, 0.518 mm thick; Rossman and Aines (1991)	Gross88Andr12
Grossular GRR 1430.2	Belvidere Mountain, Eden Mills, Vermont (F. Allen)	Moderate orange crystals, 1.381 mm thick; Rossman and Aines (1991)	Gross94Andr06
Grossular GRR 1444	Pietra Massif, Montalto di Castro, Viterbo, Lazio, Italy (E. Passaglia)	Katoite, micro KBr pellet; Passaglia and Rinaldi (1984)*; Rossman and Aines (1991)	$Ca_{2.96}(Al_{1.85}Mg_{0.01})(Si_{0.69}S_{0.11})O_{2.93}(OH)_{9.07}$*
Andradite GRR 1263	San Benito Co., CA, U.S.A. (collected by G.R. Rossman)	Black, serpentinite, 0.260 mm; Amthauer and Rossman (1998)	Andr99
Andradite 4282	Madagascar? (eBay – Zoultier.com)	Light green transparent crystal, anisotropic, 0.606 mm; Geiger et al. (2018)	Andr99
Grossular-Andradite 6741	Africa (eBay)	Greenish yellow, Anisotropic sector zoning and bands observed under crossed, 0.617 mm; Dachs and Geiger (2019)	Gross73Andr23
Andradite-Grossular KPK 56–12-9	Phu Kha Hill, Mueang District, Lop Buri Province, Thailand (IR results B. Phichaikamjornwut)	Yellowish green to brownish green, 0.5–3 mm diameter crystals, skarn; Phichaikamjornwut et al. (2012)	Andr73Gross26
Synthetic Hydrogarnet	(B. Lothenbach)	Very fine-grain; Dilnesa et al. (2014)	$Ca_3Al_2(SiO_4)(O_4H_4)_2$
Synthetic Hydrogarnet	(B. Lothenbach)	Very fine-grain; Dilnesa et al. (2014)	$Ca_3(Al_{1.4},Fe^{3+}_{0.6})_2(SiO_4)(O_4H_4)_2$
Synthetic Hydrogarnet	(B. Lothenbach)	Very fine-grain; Dilnesa et al. (2014)	$Ca_3(Al_{1.0},Fe^{3+}_{1.0})_2(SiO_4)(O_4H_4)_2$
Synthetic Hydrogarnet	(B. Lothenbach)	Very fine-grain; Dilnesa et al. (2014)	$Ca_3(Al_{0.6},Fe^{3+}_{1.4})_2(SiO_4)(O_4H_4)_2$
Synthetic Hydrogarnet	(B. Lothenbach)	Very fine-grain; Dilnesa et al. (2014)	$Ca_3Fe^{3+}_2(SiO_4)_{0.75}(O_4H_4)_{2.25}$

Infrared spectra of synthetic hydrogarnet powders (courtesy of B. Lothenbach to CAG) were obtained on a Nicolet iS50 FTIR spectrometer with the ATR method using a SensIR Technologies DuraScope diamond ATR accessory. Before each measurement, the diamond crystal was cleaned with ethanol, and the diamond surface was fully covered with sample powder that was pressed against the diamond with a rod that was terminated in aluminum foil. All spectra were corrected with a built in ATR correction that compensated for the penetration depth of the IR radiation into the sample as a function of wavelength.

Spectral results were curve-fitted using the WiRE program of Renishaw that is part of their Raman systems. Spectra with sloping baselines were first manually baseline-corrected using WiRE.

RESULTS

IR spectra (see figures detailed later) from our latest measurements, as well as some taken from the literature, will be shown in the course of the discussion (see also Part II, Geiger and Rossman 2020b, where, for example, H_2O contents of various water-poor nominally anhydrous garnets are given and discussed). Several words regarding OH^- mode wavenumbers are in order. Because different IR spectrometers with differing experimental setups were used to measure the spectra of the various garnets analyzed here,

there can be a slight variation in the wavenumber for a certain mode. In addition, the curve fits of a spectrum give the peak center wavenumber, whereas other spectra give the wavenumber at the peak maximum. Fit results also may depend slightly on several factors such as the nature of the baseline correction and band overlap, for example. All these factors lead to slight variations in the precise wavenumber for a given OH^- mode. We think, in general, that the uncertainty is better than ±2 cm^{-1} and possibly in some cases within ±1 cm^{-1}.

We note, further, that our spectral fits are subjective to a certain degree. The issue is complex, in detail, because some spectra contain a fairly large number of modes and band overlap is present. Moreover, there can be considerable differences in band intensities.

Discussion

An understanding of the IR spectra of most natural, water-bearing nominally anhydrous "end-member" garnet species, and especially intermediate solid-solution compositions, in terms of assigning observed OH^- stretching modes, is not at hand (we use quotation marks around the term end-member, because the presence of any amount of OH^- must cause deviations from exact garnet stoichiometry and also because most natural garnets are never compositionally "pure" and stoichiometric).

At this point, with respect to silicate garnets, only certain "end-member" andradite crystals are understood in terms of their OH^- incorporation at least at the first level. They represent the simplest IR spectroscopic case and both natural and synthetic crystals can apparently contain a hydroandradite component, $Ca_3Fe^{3+}_2H_{12}O_{12}$ (Geiger and Rossman 2018), via the presence of local and isolated $(H_4O_4)^{4-}$ groups. The vibrational spectrum of synthetic $Ca_3Al_2H_{12}O_{12}$ is also—at least down to about 80 K—well described and understood (Kolesov and Geiger 2005). Our analysis in this study builds upon the conclusions of our earlier work, which proposed criteria to identify the hydrogarnet substitution in terms of IR and Raman spectra and primarily in anhydrous nominally end-member garnets.

We concentrate our efforts in this Part I on the four-component system shown in Figure 1, where the currently accepted garnet terminology is taken from Grew et al. (2013). The IR spectra of these garnets are rich and complex in terms of the number of different energy OH^- bands (or "band patterns") that they exhibit (e.g., Rossman and Aines 1986; Rossman and Aines 1991; Armbruster and Geiger 1993; Amthauer and Rossman 1998; Withers et al. 1998; Maldener et al. 2003; Kurka et al. 2005; Phichaikamjornwut et al. 2012; Dachs et al. 2012; Dilnesa et al. 2014; Reynes et al. 2018). The observed OH^- bands have not been assigned, and relatively little is understood in terms of the detailed vibrational and crystal-chemical behavior. Before an analysis of the IR results can begin, it is first necessary to describe the crystal chemistry of garnet and understand what vibrational spectra of crystals measure.

Garnet crystal chemistry, general OH^--stretching mode behavior, and stability of the hydrogarnet substitution

Vibrational spectroscopy, here IR and Raman, measures local vibrations of atoms and atomic groups in molecules and crystals (Nakamoto 2009). The IR and Raman spectra of different silicate garnet species and intermediate composition solid solutions in the energy region of the lattice vibrations (1200 to 100 cm^{-1}) have been measured and analyzed based on their crystal chemistry (e.g., Moore et al. 1971; Hofmeister and Chopelas 1991; McAloon and Hofmeister 1993; Kolesov and Geiger 1998; Geiger 1998). The crystal-structure properties of various garnets have been investigated and described many times and in great detail, as made possible by a multitude of diffraction studies (e.g., Novak and Gibbs 1971; Armbruster and Geiger 1993; Geiger and Armbruster 1997).

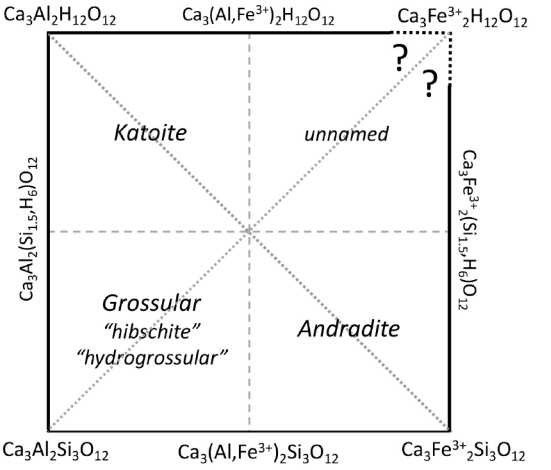

Figure 1. The four-component system $Ca_3Al_2H_{12}O_{12}$–$Ca_3Fe^{3+}_2H_{12}O_{12}$–$Ca_3Fe^{3+}_2Si_3O_{12}$–$Ca_3Al_2Si_3O_{12}$ and the respective garnet nomenclature. The thick solid black lines indicate the degree of possible solid solution and the black dotted lines indicate uncertainty. There can be complete solid solution along the andradite-grossular and grossular-katoite binaries, but the full degree of solid solution along the $Ca_3Fe^{3+}_2H_{12}O_{12}$-andradite and katoite-$Ca_3Fe^{3+}_2H_{12}O_{12}$ joins is not known. The two gray dashed lines mark the 50:50 compositions of the four binary systems. The solid-solution behavior of the $Ca_3Fe^{3+}_2Si_3O_{12}$-$Ca_3Al_2H_{12}O_{12}$ and $Ca_3Al_2Si_3O_{12}$-$Ca_3Fe^{3+}_2H_{12}O_{12}$ binaries (gray dotted lines), as well as higher-order ternary or quaternary compositions, is also not understood.

Consider the local crystal chemistry around the crystallographic Wyckoff 24*d* position, space group $Ia\bar{3}d$, and the cation-oxygen bonding arrangement. The (*Z*) cation at 24*d,* site symmetry –4, is Si^{4+} for most natural garnets. In garnet containing a hydrogarnet component, a Si^{4+} atom is absent and proxied locally by four H^+ (or D^+) atoms, as shown by several neutron diffraction investigations (Cohen-Addad et al. 1967; Foreman 1968; Lager et al. 1987; Lager and von Dreele 1996). The protons bisect and lie slightly above the four surfaces of a tetrahedron that is defined by four oxygen atoms to which they are bonded with an OH^- bond length of 0.906(2)/0.925(12) Å (Lager and von Dreele 1996). The crystallographic positions of the four H^+ cations result from the atomic forces acting in the garnet and the necessity to maintain *local charge balance* in the vicinity of the 24*d* site. Crystallographically, there is just a single O atom located at a general position (*x*,*y*,*z*) in garnet. Thus, there are just single OH^- groups that vibrate and there are no $(H_4O_4)^{4-}$-type vibrations. There are only individual OH^--stretching vibrations in the energy region around 3600 ± 100 cm^{-1} (Kolesov and Geiger 2005; Orlando et al. 2006). There is little reason to consider $(H_4O_4)^{4-}$-group-like vibrations (i.e., Harmon et al. 1982), because they should not exist. This is a good reason to express the general formula of hydrogarnets as $\{X_3\}[Y_2](H_{12})O_{12}$. Furthermore, it has been argued that there is very weak, if any,

hydrogen bonding present (cf. Harmon et al. 1982; Orlando et al. 2006; Geiger and Rossman 2018). Thus, this potential complication to OH^- vibrational behavior can probably be ignored, based on the existing results.

The relevant local atomic configuration is shown in Figure 2. The H^+ atom is bonded to a single oxygen atom that is also chemically bonded to a single *Y*-cation (Wyckoff 16*a* position) and two *X*-cations (Wyckoff 24*c* position) with different *X*-O chemical bond lengths. Because of this arrangement, there must be OH^--mode coupling and/or mixing with *Y*- and *X*-cation-related vibrations. For the common silicate garnets, *X* can be Ca, Mg, Fe^{2+}, and Mn^{2+} and *Y* can be Al^{3+}, Fe^{3+}, and Cr^{3+} and they can exchange with one another to various degrees at the *X*- and *Y*-sites, respectively, giving a range of compositionally complex substitutional solid solutions (Geiger 2008). There are considerable differences in ionic radii, masses, and electronic states among these various cations and, therefore, the associated chemical bonds must be different in nature.

Adopting a harmonic oscillator to describe the vibration of an atom pair (*A* and *B*), the frequency is given by:

$$v = \frac{1}{2\pi}\sqrt{\frac{k}{\mu_{AB}}} \quad (1)$$

where *k* is the force constant (i.e., in simple terms the bond strength) and μ_{AB} is the reduced mass of the system [$\mu_{AB} = (m_A m_B)/(m_A + m_B)$]. It is obvious that an O-H stretching mode will have a different vibrational frequency depending on the precise local atomic configuration and the nature of the various chemical bonds involving the common oxygen atom (Fig. 2) and also possibly beyond. Geiger and Rossman (2018) discussed the case for various OH^--bearing "end-member" garnet species. They all show a single OH^- stretching mode at RT whose energy is a function of the atomic masses and strengths of the different chemical bonds of the "extended vibrational system." The greater the mass, the lower will be the wavenumber of the OH^- stretching mode, ignoring other factors.

This reasoning explains, for example, the lower energy of the OH^- stretching mode in the IR spectra (Albrecht et al. 2019) of the synthetic hydrogarnets $Ca_3Cr_2^{3+}H_{12}O_{12}$, $Sr_3Cr_2^{3+}H_{12}O_{12}$ and $Ca_3Rh_2^{3+}H_{12}O_{12}$ (i.e., 3616, 3625, and 3592 cm^{-1}, respectively) compared to that for $Ca_3Al_2H_{12}O_{12}$ (i.e., 3662 cm^{-1}). The OH^- stretching mode, observed in RT spectra, is generally broad in OH^--bearing end-member garnets because of the large vibrational amplitudes of the H^+ atom (Lager et al. 1987). Cooling the crystal dampens significantly the amplitudes of vibration and the single OH^- band at RT narrows greatly and ultimately at about 80 K or slightly below two modes are observable in IR spectra (Kolesov and Geiger 2005; Geiger and Rossman 2018).

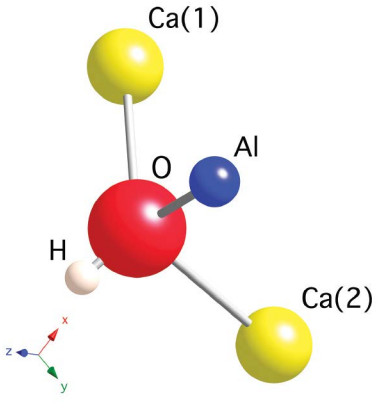

FIGURE 2. Local atomic environment involving a single OH^- dipole in the case of calcium hydrogarnet (no Si cation). The oxygen anion (red) is bonded to one *Y* (Al or Fe^{3+}) cation (blue), two *X* (Ca) cations (yellow) with bond lengths of Ca1-O = 2.462(3) Å and Ca(2)-O = 2.520(3) Å in hydrogrossular (Lager et al. 2002) and a H atom (pink). (Color online.)

Of course, pure, end-member composition silicate garnets are rare, if they even exist in nature. There is almost always some degree of cation mixing at the *X*- and *Y*-sites. This means there can be various local cation configurations around a given oxygen atom in a solid-solution crystal (Fig. 2). Their concentration depends on the garnet bulk composition. The precise local crystal-chemical situation (i.e., atomic order-disorder and structural relaxation) is complex, and it is not fully understood at this time. Suffice it to say, here, that the intensities of the different OH^- stretching modes will depend on the relative amounts of the various local cation configurations. Different vibrational possibilities could exist in a solid-solution garnet. One is that each local atomic configuration will result in a representative OH^- mode with its characteristic energy, as in the respective "end-member" garnets grossular, andradite or katoite, for example. Another possible behavior is that a distribution of relatively closely spaced OH^- modes, each with not too different energies, occurs. This latter situation can give rise to OH^--band broadening and varying the temperature of the IR measurement will not significantly affect OH^- band widths. This effect is called chemical-mode broadening in comparison to pure vibrational-mode broadening. In terms of many natural OH^--bearing garnets both can occur.

Finally, it must be stressed, as a key basis for our analysis, that the substitution $(H_4O_4)^{4-} \leftrightarrow (SiO_4)^{4-}$ or $(H_4)^{4+} \leftrightarrow (Si)^{4+}$ is energetically favorable for grossular-katoite crystals, as shown by synthesis experiments (Flint et al. 1941; Carlson 1956; Kobayashi and Shoji 1983) and also to a large, but not complete, degree in $Ca_3Fe_2^{3+}(SiO_4)_3$-$Ca_3Fe_2^{3+}(H_4O_4)_3$ garnets (Flint et al. 1941; Dilnesa et al. 2014). No other common silicate binary garnet system shows such a complete exchange. Phase equilibrium studies on $Ca_3Al_2(SiO_4)_3$-$Ca_3Al_2(H_4O_4)_3$ solid solutions at high *P* and *T* under hydrothermal conditions indicate that thermal stability increases with decreasing H_2O in the garnet (Yoder 1950; Pistorius and Kennedy 1960). Finally, empirical pair potential calculations show that the reaction grossular + water → katoite is thermodynamically favored (Wright et al. 1994).

A simple question is then: why are the IR spectra of nominally anhydrous grossular and other calcium silicate garnets so variable and complex compared to those of other natural silicate garnets (e.g., pyrope, almandine, spessartine) in terms of their OH^- incorporation?

IR spectra, OH^- stretching modes and their assignment, hydrogarnet domains and clusters

Katoite and water-rich katoite-grossular solid solutions. We start our analysis with synthetic end-member katoite, $Ca_3Al_2H_{12}O_{12}$, with a well-known crystal structure (Cohen-Addad et al. 1967; Foreman 1968; Lager et al. 1987) and IR and Raman spectrum (Kolesov and Geiger 2005). At RT, its IR spectrum shows a broad,

single asymmetric OH^- stretching mode at 3662 cm^{-1}. It can be fit with two components with energies of about 3681 and 3666 cm^{-1} at about 80 K. At even lower temperatures, both the IR and Raman spectra become complex in the OH^- stretching region with the appearance of many new, weak OH^- modes, but this aspect is not considered further here. The OH^- "doublet" at roughly 80 K is asymmetric, whereby the higher energy OH^- band is considerably more intense than the lower energy one. Geiger and Rossman (2018) argued that this spectroscopic behavior of OH^--mode splitting characterizes the hydrogarnet substitution in most "end-member" silicate garnets.

Consider now the IR single-crystal spectra of intermediate $Ca_3Al_2Si_3O_{12}$-$Ca_3Al_2H_{12}O_{12}$, both natural and synthetic, garnets (Fig. 3, replotted from Rossman and Aines 1991) containing major H_2O contents. From these five spectra it is immediately apparent that the band at about 3660 cm^{-1} does not vary greatly in wavenumber, but it decreases in intensity with an increasing number of Si atoms in the formula unit (or grossular component). We conclude, therefore, that this mode must represent the presence of katoite-like domains in the solid-solution composition garnets. [A strong OH^- band at 3660 cm^{-1}, as well as a couple of others with high wavenumber, was observed in the IR powder in KBr spectra of a series of synthetic $Ca_3Al_2Si_3O_{12}$-$Ca_3Al_2H_{12}O_{12}$ garnets (Kobayashi and Shoji 1983). However, the quality of the published spectra does not permit a precise analysis.] The local crystal-chemical situation is shown in Figure 4a.

It can also be observed in a couple of IR spectra (GRR 1329 and GRR 1358) that there is a strong OH^- band between 3595 and 3660 cm^{-1} that increases in intensity with increasing grossular component in the solid solution (Fig. 3). Rossman and Aines (1991) wrote in their IR study of grossular garnets, "We assign the band at 3598 cm^{-1}, which is dominant in the silica-rich hydrogrossular samples, to $(O_4H_4)^{4-}$ groups, adjacent to SiO_4 groups." We accept this proposal. The local crystal-chemical situation is illustrated in Figure 4b and it shows a single, isolated $(H_4O_4)^{4-}$ group imbedded in an anhydrous grossular "matrix." The wavenumber of the associated OH^- mode is about 60 cm^{-1} less than in end-member katoite and could be a function of two effects. The first is related to bond strengths. In end-member grossular the two different Ca-O bond lengths (Fig. 2) are Ca(1)-O(4) = 2.322(1) Å and Ca(2)-O(4) = 2.487(1) Å (Geiger and Armbruster 1997). They are shorter, and thus stronger, than in end-member katoite, where Ca(1)-O(4) = 2.465(2) Å and Ca(2)-O(4) = 2.511(1) Å (Lager et al. 1987). It can be expected that local Ca-O bonds in water-bearing grossular vary in length depending on the precise structural state within a solid solution. Stronger Ca-O bonds translate to weaker O-H bonds (Geiger and Rossman 2018). Second, it could be expected that there is extended mode coupling and/or mixing beyond the fragment shown in Figure 2 that affects O-H bonding. The presence of heavier Si^{4+} cations compared to H^+ atoms in a garnet solid solution could act to lower the OH^- stretching vibration energy.

The IR and Raman spectra indicate, therefore, two "end-member type" $(H_4O_4)^{4-}$ substitution mechanisms. Obvious questions arise however. One is apparent in the spectrum of garnet GRR 1058 (Fig. 3). The broad OH^- mode envelope has structure and shows a peak maximum at roughly 3620 cm^{-1}. How is it to be assigned? More generally, published IR spectra of water-poor grossulars show a varying number of OH^- bands located between

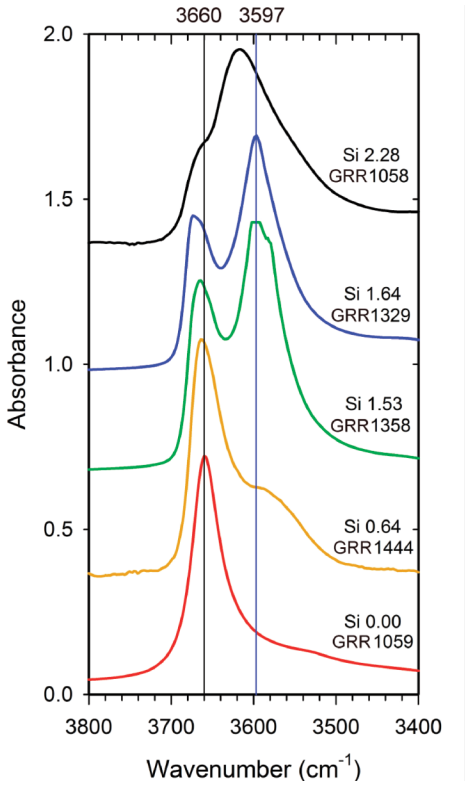

FIGURE 3. IR single-crystal spectra in the energy range of the OH^- stretching vibrations for five natural and synthetic garnets along the join $Ca_3Al_2(H_4O_4)_3$-$Ca_3Al_2(SiO_4)_3$ as replotted from Rossman and Aines (1991). The sample labels (Table 1) and the number of Si atoms per formula unit (pfu) are given. (Color online.)

3660 and 3600 cm^{-1}. How are they to be assigned?

"End-member" or nearly end-member grossular. To answer these questions, we consider the IR spectra of several "end-member" or closely end-member composition grossulars, both synthetic and natural. The spectra of a hydrothermally synthesized grossular (Geiger and Armbruster 1997, grown from the oxides CaO from $CaCO_3$, Al_2O_3, and SiO_2) and a nearly end-member composition natural garnet (GRR 53, Table 1) are shown together in Figure 5a. The two spectra are remarkably similar in appearance and give the first "spectroscopic match" between a synthetic and a natural crystal [We interject, here, that the IR powder spectra on synthetic grossular recorded by Hsu (1980) show weak absorption features at about 3620 and 3660 cm^{-1} that could be interpreted as indicating structural OH^-, as well as a broad and intense absorption band centered at 3420 cm^{-1} that can be assigned to liquid water. It is our experience, though, that IR powder spectra are normally insufficient for characterizing precisely small amounts of OH^- in minerals.] The spectra of both the synthetic crystal and GRR 53 show three intense OH^--bands at 3666, 3633, and 3623 cm^{-1}. Consider, furthermore, the IR spectra of the synthetic and natural grossulars shown in Figure 6. They show different OH^- spectral features from those garnets in Figure 5a and have intense modes at 3623 (±1) and 3603 cm^{-1}. The two garnets give a second spectral "match" between a synthetic and natural end-member composition crystal.

The spectrum of the synthetic grossular in Figure 5a shows

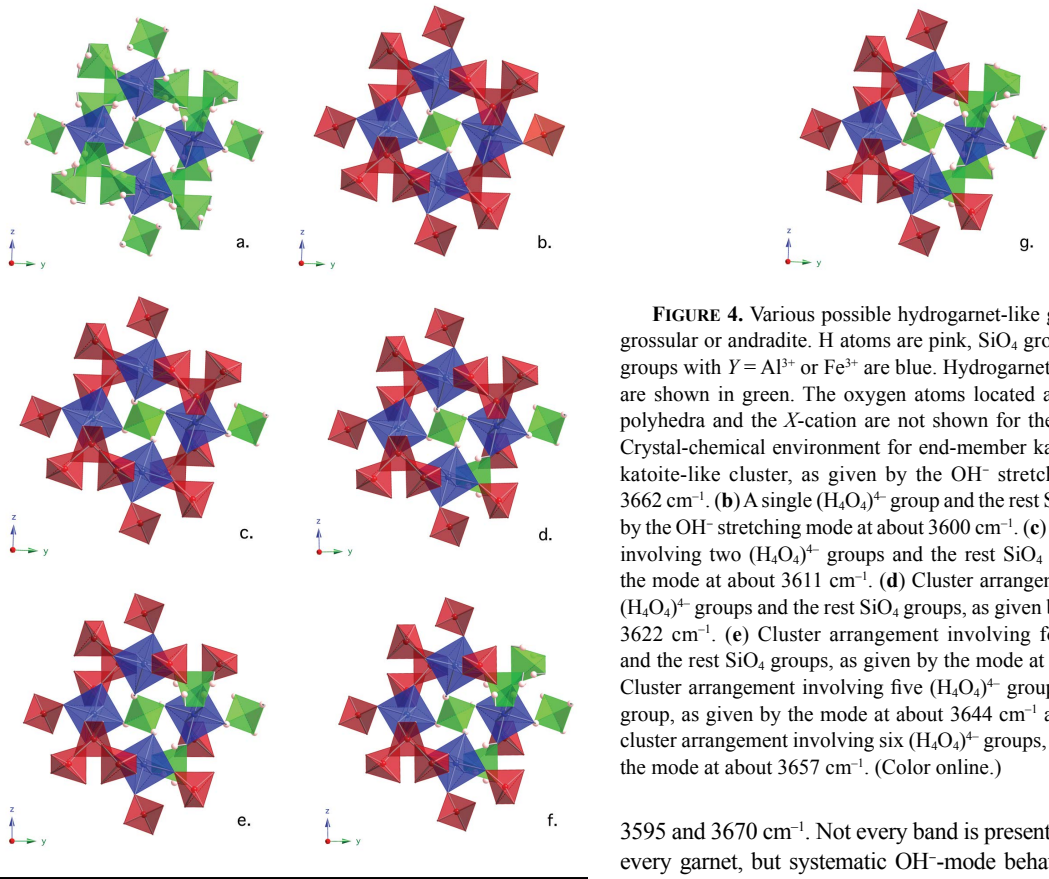

FIGURE 4. Various possible hydrogarnet-like groups or clusters in grossular or andradite. H atoms are pink, SiO_4 groups are red and YO_6 groups with $Y = Al^{3+}$ or Fe^{3+} are blue. Hydrogarnet (H_4O_4) "tetrahedra" are shown in green. The oxygen atoms located at the corners of the polyhedra and the *X*-cation are not shown for the sake of clarity. (**a**) Crystal-chemical environment for end-member katoite or a finite-size katoite-like cluster, as given by the OH^- stretching mode at about 3662 cm^{-1}. (**b**) A single $(H_4O_4)^{4-}$ group and the rest SiO_4 groups, as given by the OH^- stretching mode at about 3600 cm^{-1}. (**c**) Cluster arrangement involving two $(H_4O_4)^{4-}$ groups and the rest SiO_4 groups, as given by the mode at about 3611 cm^{-1}. (**d**) Cluster arrangement involving three $(H_4O_4)^{4-}$ groups and the rest SiO_4 groups, as given by the mode at about 3622 cm^{-1}. (**e**) Cluster arrangement involving four $(H_4O_4)^{4-}$ groups and the rest SiO_4 groups, as given by the mode at about 3633 cm^{-1}. (**f**) Cluster arrangement involving five $(H_4O_4)^{4-}$ groups and a single SiO_4 group, as given by the mode at about 3644 cm^{-1} and (**g**) Hypothetical cluster arrangement involving six $(H_4O_4)^{4-}$ groups, as possibly given by the mode at about 3657 cm^{-1}. (Color online.)

fine structure (e.g., shoulders on the main peaks) indicating the presence of additional OH^- modes and, therefore, it was curve fit to describe them (Fig. 5b). Additional bands at 3688, 3660, 3645, 3613, 3604, 3578, and 3561 cm^{-1} result. This gives a total of 10 possible OH^- modes for this synthetic grossular. We analyze and assign them. First, however, we note that the weak modes at 3561, 3579, and 3688 cm^{-1} may be experimental artifacts arising from the difficultly in collecting a spectrum with a smooth baseline on the tiny synthetic crystal. On the other hand, they could also be real and possible assignments are discussed below. Summarizing for the present discussion, this gives seven OH^- modes at about 3666, 3660, 3645, 3633, 3623, 3613, and 3604 cm^{-1}. There appears to be an approximate regularity in the wavenumber spacing between the modes.

It turns out that these OH^- modes, in various combinations and with differing intensities, are observed in most, if not all, published IR spectra of natural grossular crystals. To be sure, the large number of spectra in Rossman and Aines (1991) shows intense OH^- bands at about 3612, 3622, 3633, and 3641 cm^{-1} depending on the specific crystal in question. Indeed, the presence or absence and the intensity of these modes (i.e., the spectral pattern) were used to define or to characterize their different classes of OH^--bearing grossulars. Phichaikamjornwut et al. (2012) in their IR study of different natural grossular-andradite garnets also measured intense modes at about 3602, 3612, 3631, and 3641 cm^{-1}.

All the IR results, analyzed together, indicate a spectral systematics defined by OH^--bands with similar wavenumbers between 3595 and 3670 cm^{-1}. Not every band is present in the spectrum of every garnet, but systematic OH^--mode behavior is observable. Thus, we propose that OH^- stretching modes at about 3599, 3612, 3622, 3633, 3641, and 3657 cm^{-1} could arise from the presence of various, local hydrogrossular-like clusters occurring in an anhydrous grossular "matrix." Table 2 lists the different modes. (Note: Based on our analysis of many spectra, the mode at about 3657 cm^{-1} appears to be the most problematic in the sense that it often does not occur and/or that it is weak in intensity in the spectra of many garnets.) We have no good explanation for this, except to state that this mode is related to a six-membered $(H_4O_4)^-$ cluster—Fig. 4g—that is structurally, and thus probably energetically, similar to a katoite-like cluster—Fig. 4a—having an OH^- mode around 3660 cm^{-1}. Thus, the latter type of cluster may occur more preferentially). From this analysis, seven types of local $(H_4O_4)^{4-}$ clusters (and/or domain in the case of water-rich hydrogarnets) can be constructed by having different numbers of $(H_4O_4)^{4-}$ groups in them and they can be assigned to the different energy OH^- modes. Figures 4a–4g shows the respective atomic configurations for the different cluster types. According to our model analysis, the OH^- mode wavenumber increases with the number of $(H_4O_4)^{4-}$ groups in a given cluster.

Summarizing our analysis, the observed OH^--stretching modes between 3595 and 3670 cm^{-1} in the IR spectra for many different OH^--bearing grossulars and katoites can be interpreted and assigned in a completely new context. Figure 7 shows IR spectra, including one water-rich grossular and six water-poor samples having an intense OH^- mode at one or more of the characteristic wavenumbers. It must be noted, though, that other OH^- bands can be also observed above and below this wavenumber range. This

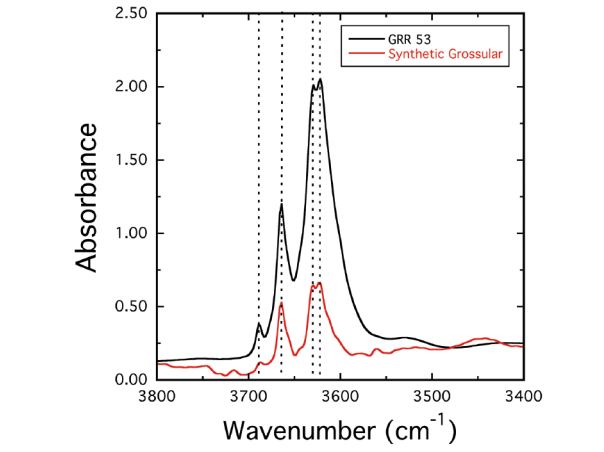

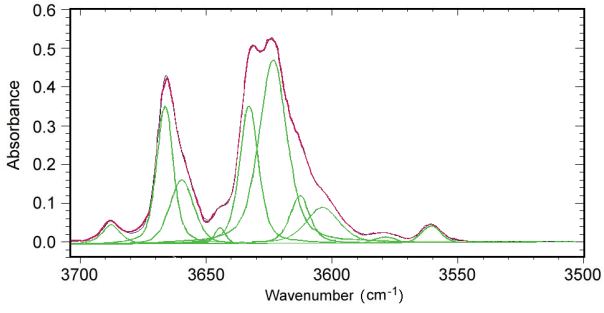

Curve Name	Centre	Width	Height	% Gaussian	Type	Area
Curve 1	3688	8.2	0.05	26	Mixed	0.59
Curve 2	3666	7.7	0.36	58	Mixed	3.51
Curve 3	3660	11.2	0.17	72	Mixed	2.26
Curve 4	3645	5.4	0.04	100	Mixed	0.24
Curve 5	3633	8.9	0.36	56	Mixed	4.08
Curve 6	3623	13.1	0.48	52	Mixed	8.14
Curve 7	3613	9.1	0.12	51	Mixed	1.46
Curve 8	3604	15.4	0.09	54	Mixed	1.85
Curve 9	3579	9.8	0.02	100	Mixed	0.16
Curve 10	3561	8.8	0.04	82	Mixed	0.44

FIGURE 5. (**a**) IR single-crystal spectra in the wavenumber range of the OH^- stretching vibrations at RT of synthetic "end-member" grossular normalized to 1 mm thickness (Geiger and Armbruster 1997) and natural nearly end-member grossular GRR 53 (Table 1). (**b**) Fitted spectrum of synthetic grossular. (Color online.)

aspect is now considered.

Other possible OH^- substitution mechanisms in "end-member" grossular and hydrous inclusions. The IR spectra of water-poor natural grossular can often show OH^- bands that are not listed above and lie at energies above 3670 cm^{-1}. Their assignments are not known and remain to be made. Consider, first, the high-energy OH^- mode at 3684–3688 cm^{-1} at RT that has often been observed (Fig. 8 and see spectra in Rossman and Aines 1991; Kurka et al. 2005; Dachs et al. 2012; Phichaikamjornwut et al. 2012). This mode has stronger O-H bonding compared to those OH^- bands between 3595 and 3662 cm^{-1} and it cannot be assigned based on the model analysis given above. One speculative possibility is that it arises from the substitution $\{2H^+ \leftrightarrow Ca^{2+}\}$. A H^+ atom, as part of an OH^- dipole directed toward the interior of an *X*-cation-free (site 24*d*) oxygen coordinated dodecahedron, should have relatively little interaction with other atoms in the garnet structure. It could be expected to be the "freest OH^- dipole" of any in grossular and thereby have the strongest O-H bond.

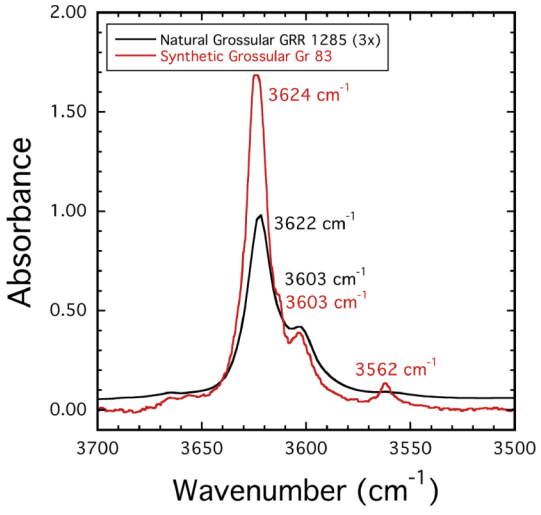

FIGURE 6. IR single-crystal spectra in the energy range of the OH^- stretching vibrations at RT of natural grossular GRR 1285 (intensity 3×) and synthetic grossular Gr83 (normalized to 1 mm thickness) of Withers et al. (1998). Samples described in Table 1. (Color online.)

Alternatively, this high wavenumber mode might be related to the presence of tiny inclusions of a foreign OH^--bearing phase. High wavenumber OH^- bands (greater than 3670 cm^{-1}) in the spectra of andradite and pyrope have been argued to be due to the presence of inclusions of minute layer silicates such as talc and phlogopite (Geiger et al. 2018; Geiger and Rossman in review). What about grossular? The spectra of serpentine minerals (i.e., chrysotile, lizardite, antigorite) are characterized by OH^- bands with high energies. Schroeder (2002) gives 3686 cm^{-1} for the strong OH^- band for the spectrum of lizardite and Mellini et al. (2002) measured 3684 cm^{-1} for lizardite from Elba Island. Band energies depend on the precise compositions of the phases (Heller-Kallai et al. 1975). The absorption features can be broad in nature and show fine structure and are variable depending on the precise serpentine mineral. A band at about 3674–3677 cm^{-1} can also be observed in some spectra of grossular (Fig. 8). Antigorite can show a strong OH^- band (asymmetric in shape) with a peak maxima of 3674–3678 cm^{-1} (Heller-Kallai et al. 1975; Mellini et al. 2002). Talc, as well, shows an intense OH^- band at 3677 cm^{-1} (Schroeder 2002). It is important to note that nearly end-member grossular crystals can often be found in rodingites associated with serpentinites (see the discussion in Part II on grossulars from Asbestos, Canada). Therefore, in light of the evidence, the high energy bands at about 3684–3688 and 3674–3677 cm^{-1} in the spectra of grossular are best assigned, at least at this time, to the presence of tiny inclusions of hydrous Mg-rich layer silicates.

In addition to these high wavenumber OH^- modes, other bands with energies less than about 3595 cm^{-1} have been observed in the spectra of many natural grossulars (Rossman and Aines 1991; Kurka et al. 2005; Phichaikamjornwut et al. 2012; Dachs et al. 2012; this work). We address them below, but first we consider the IR spectra of synthetic $Ca_3Fe^{3+}_2H_{12}O_{12}$-bearing hydrogarnet solid solutions and natural end-member andradite.

Water-rich $Ca_3Fe^{3+}_2Si_3O_{12}$-$Ca_3Fe^{3+}_2H_{12}O_{12}$-$Ca_3Al_2Si_3O_{12}$-$Ca_3Al_2H_{12}O_{12}$ solid solutions. End-member $Ca_3Fe^{3+}_2H_{12}O_{12}$

TABLE 2. OH^- stretching modes (greater than 3560 cm^{-1}) observed for calcium silicate garnets at room temperature, their assignment and cluster type

Natural grossulars[a] (cm^{-1})	Natural andradite[b] (cm^{-1})	Synthetic grossular-andradite-$Ca_3Al_2H_{12}O_{12}$-$Ca_3(Al,Fe^{3+})_2H_{12}O_{12}$ garnets (cm^{-1})	Synthetic grossular[c] (cm^{-1})	Synthetic hydro/andradite[d] (cm^{-1})	Assignment	Crystal chemistry clustertype
3684–3688	–	–	(3688)?	–	Hydrous inclusion phase	–
3674–3678	~3678	–	–	–	Hydrous inclusion phase	–
~3660	–	~3658	3666	–	Finite size katoite cluster	Fig. 4a
~3657	–	–	3660	–	Six $(H_4O_4)^{4-}$ hydrogrossular cluster (?)	Fig. 4g
~3641	–	–	3645	–	Five $(H_4O_4)^{4-}$ hydrogrossular cluster	Fig. 4f
~3634	~(3632)	–	3633	–	Four $(H_4O_4)^{4-}$ hydrogrossular cluster	Fig. 4e
~3622	~(3621)	–	3623	–	Three $(H_4O_4)^{4-}$ hydrogrossular cluster	Fig. 4d
~3612	~(3611)?	–	3613	–	Two $(H_4O_4)^{4-}$ hydrogrossular cluster	Fig. 4c
~3599	–	–	3604	–	One $(H_4O_4)^{4-}$ hydrogrossular group	Fig. 4b
–	~3611?	~3611	–	3612	Finite size $Ca_3Fe_2^{3+}O_{12}H_{12}$ cluster (?)	Fig. 4a
~(3594)	~3594	–	–	–	Unspecified hydroandradite cluster	?
~(3581)	~3581	–	(3579)?	–	Unspecified hydroandradite cluster	?
~(3563)	~3563	–	(3560)?	3563	One $(H_4O_4)^{4-}$ hydroandradite group	Fig. 4b

[a] Varies from garnet to garnet and can be absent.
[b] Geiger and Rossman (2018) and sample 4282.
[c] This work from curve fit.
[d] Geiger and Rossman (2018) and Amthauer and Rossman (1998) for synthetic $Ca_3Fe_2^{3+}(4H_{0.19}Si_{2.81})O_{12}$.

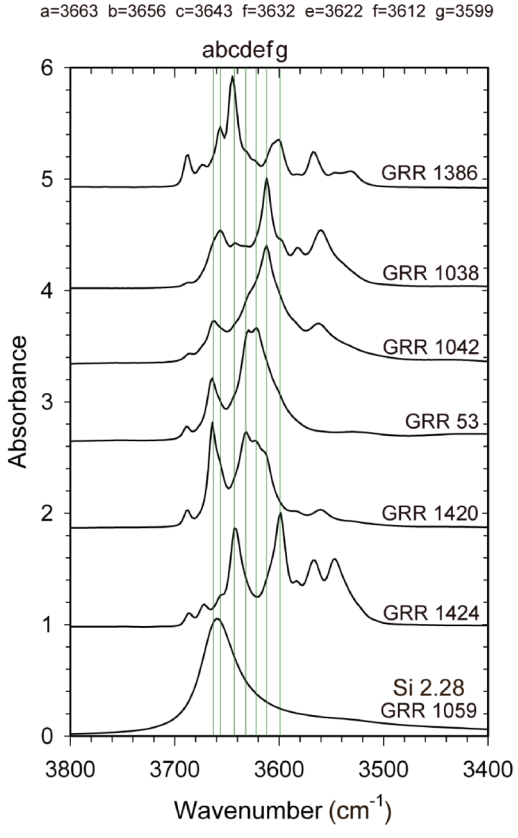

FIGURE 7. Stacked plot of different spectra of natural grossulars (Table 1) and the synthetic hydrogrossular GRR 1059 showing hydrogrossular-like OH^- modes at about 3599, 3612, 3622, 3633, 3643, 3657, and 3662 cm^{-1}. They are related to different microscopic- to nano-size hydrogarnet clusters (see text). The mode at 3688 cm^{-1} may be due to tiny "serpentine mineral" inclusions (see text). (Color online.)

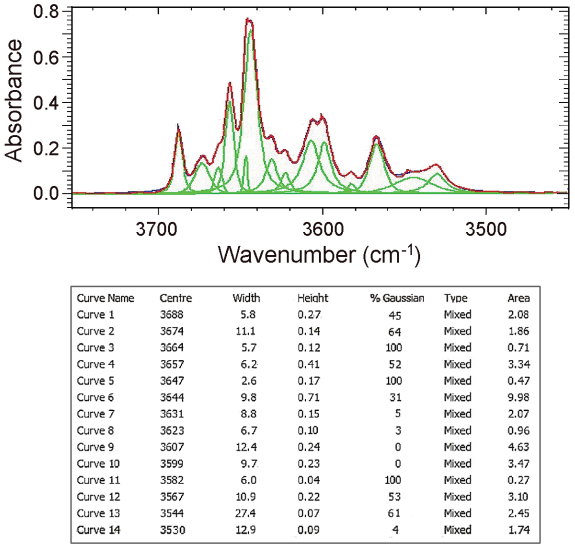

Curve Name	Centre	Width	Height	% Gaussian	Type	Area
Curve 1	3688	5.8	0.27	45	Mixed	2.08
Curve 2	3674	11.1	0.14	64	Mixed	1.86
Curve 3	3664	5.7	0.12	100	Mixed	0.71
Curve 4	3657	6.2	0.41	52	Mixed	3.34
Curve 5	3647	2.6	0.17	100	Mixed	0.47
Curve 6	3644	9.8	0.71	31	Mixed	9.98
Curve 7	3631	8.8	0.15	5	Mixed	2.07
Curve 8	3623	6.7	0.10	3	Mixed	0.96
Curve 9	3607	12.4	0.24	0	Mixed	4.63
Curve 10	3599	9.7	0.23	0	Mixed	3.47
Curve 11	3582	6.0	0.04	100	Mixed	0.27
Curve 12	3567	10.9	0.22	53	Mixed	3.10
Curve 13	3544	27.4	0.07	61	Mixed	2.45
Curve 14	3530	12.9	0.09	4	Mixed	1.74

FIGURE 8. IR spectrum of grossular GRR 1386 (Table 1) and its curve fit. Note the OH^- modes at 3688 and 3674 cm^{-1}. They are possibly related to the presence of tiny inclusion phases of hydrous layer silicates and probably a "serpentine mineral" (see text). (Color online.)

has yet to be synthesized and, therefore, its OH^- mode energy cannot be measured directly, as was done with $Ca_3Al_2H_{12}O_{12}$. However, water-rich hydrogarnets in the four-component system $Ca_3Fe_2^{3+}Si_3O_{12}$-$Ca_3Fe_2^{3+}H_{12}O_{12}$-$Ca_3Al_2Si_3O_{12}$-$Ca_3Al_2H_{12}O_{12}$ have been synthesized (Dilnesa et al. 2014). Thus, we made IR ATR powder measurements on five garnets of nominal composition $Ca_3Al_2(Si_{1.0},H_{8.0})O_{12}$, $Ca_3[Al_{1.4},Fe_{0.6}^{3+}]_2(Si_{1.0},H_{8.0})O_{12}$, $Ca_3[Al_{1.0},Fe_{1.0}^{3+}]_2(Si_{1.0},H_{8.0})O_{12}$, $Ca_3[Al_{0.6},Fe_{1.4}^{3+}]_2(Si_{1.0},H_{8.0})O_{12}$, and $Ca_3[Fe_{2.0}^{3+}](Si_{0.75},H_{9.0})O_{12}$ (Table 1). The spectra are shown in Figure 9. Two main absorption features occur at 3611 and 3658 cm^{-1}. We think these two energies describe the presence of $Ca_3Fe_2^{3+}H_{12}O_{12}$- and $Ca_3Al_2H_{12}O_{12}$-like domains in these garnets, respectively. The latter mode energy agrees with the spectroscopic results discussed above. Spectral variations as a function of garnet composition are apparent. The OH^- mode (expressed as a band or a shoulder) at about 3658 cm^{-1} decreases in relative intensity with decreasing $Ca_3Al_2H_{12}O_{12}$ component in the garnet, as expected.

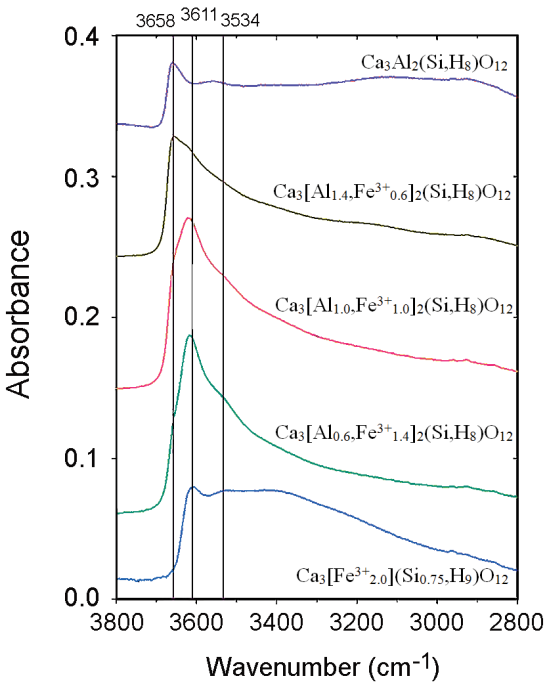

Figure 9. Stacked plot of IR ATR powder spectra of five synthetic hydrogarnets as synthesized and described by Dilnesa et al. (2014). (Color online.)

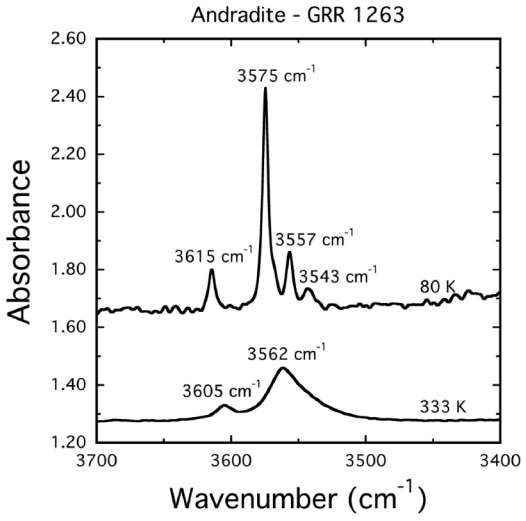

Figure 10. IR single-crystal spectra in the energy range of the OH^- stretching vibrations at 333 and 80 K of a natural "end-member" andradite GRR 1263 (Table 1).

Concurrently, the OH^- mode at 3611 cm^{-1} increases in relative intensity with increasing $Ca_3Fe^{3+}_2H_{12}O_{12}$ component in the garnet (Fig. 9)—there also appears to be a weaker OH^- mode at about 3534 cm^{-1} in the spectra of these garnets, but it should have another origin and is not considered in this work.

"End-member" or nearly end-member andradite. The RT IR single-crystal spectra of several "end-member" andradites have been recorded (Amthauer and Rossman 1998; Adamo et al. 2011; Zhang et al. 2015; Geiger et al. 2018). The low-temperature IR spectra of several natural crystals and one synthetic were measured down to 80 K by Geiger and Rossman (2018). The IR spectra of most, but not all, "end-member" andradites are simpler compared to the situation for grossular in terms of the number of observed OH^- modes. Many spectra of andradite contain just one or two OH^- modes at RT. Most natural and hydrothermally synthesized crystals show the most intense OH^- band, which is broad and asymmetric, at or near 3563 cm^{-1}. It splits into two bands at 3575 and 3557 cm^{-1} at 80 K (Geiger and Rossman 2018). Or it possibly splits into three modes, including the one at 3543 cm^{-1} for andradite GRR 1263 (Fig. 10 and Table 1). At any rate, we consider these bands to represent the presence of single, isolated $(H_4O_4)^{4-}$ groups (Fig. 4b) in andradite (Table 2).

The lower OH^- stretching energy compared to the analogous situation for single, isolated $(H_4O_4)^{4-}$ groups in grossular is largely due to the fact that the mass of Fe^{3+} (55.85 amu) is twice that of Al^{3+} (26.98 amu). Equation 1 describes the general situation. The mass effect is clearly demonstrated by the energies of the IR-active translational (T) vibrations of both cations in garnet. The wavenumber range for $T(Fe^{3+})$ modes lies between 130 and 360 cm^{-1} for andradite and for $T(Al^{3+})$ modes in grossular between about 240 and 470 cm^{-1} (McAloon and Hofmeister 1993).

Other higher wavenumber OH^- bands can be observed in the spectra of some water-poor andradites such as that shown in Figure 9 as given by the mode at 3605 cm^{-1} at 333 K. Moreover, an OH^--band with a wavenumber of 3612 (±1) cm^{-1} can be observed as part of a very broad OH^- absorption feature in the RT spectra of andradite crystals that contain a significant amount of the $Ca_3Fe^{3+}_2H_{12}O_{12}$ component (see Fig. 2 in Amthauer and Rossman 1998). We propose that the OH^- band at roughly 3612 cm^{-1} at RT in andradite-rich garnets (Table 2) could be related to the presence of finite-sized $Ca_3Fe^{3+}_2O_{12}H_{12}$-like clusters (Fig. 4a).

Finally, we propose, because andradite and grossular are so similar structurally that, in an analogous manner to the situation discussed above for hydrogrossular-like clusters in water-poor grossular, a series of different hydroandradite-like clusters may be present in some andradite crystals. They should be characterized by having OH^- stretching modes with energies between 3563 and 3606–3612 cm^{-1}. Consider, for example, the RT IR spectrum of "end-member" andradite 4282 (Fig. 11) that contains only 0.02 wt% Al_2O_3 (Geiger et al. 2018, see also a similar spectrum of andradite in Zhang et al. 2015). It is "untypical." Starting with the intense mode at 3561 cm^{-1} and moving to higher wavenumbers, one observes two OH^- modes at 3582 and 3595 cm^{-1}. We think they could represent the presence of two different hydroandradite-like clusters, whose exact $(H_4O_4)^{4-}$-group configuration (Figs. 4c–4f) cannot be presently determined. Finally, in terms of this andradite garnet, the three modes at 3610, 3621, and 3633 cm^{-1} can be assigned to three hydrogrossular-like-clusters (Table 2).

We close this section by noting that many andradites and grossulars are not of "end-member" composition. There is often some degree of solid solution between the two and also to a lesser degree with other common garnet components (e.g., $Fe^{2+}_3Al_2Si_3O_{12}$, $Mn^{2+}_3Al_2Si_3O_{12}$, $Mg_3Al_2Si_3O_{12}$). To address the issue of OH^- incorporation in calcium silicate garnets more fully, we need to consider the IR spectra of water-poor intermediate composition grossular-andradite crystals.

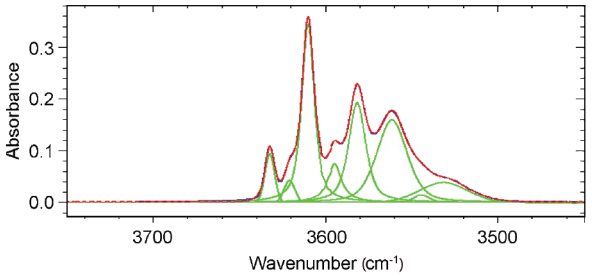

Curve Name	Centre	Width	Height	% Gaussian	Type	Area
Curve 1	3633	6.6	0.10	100	Mixed	0.67
Curve 2	3621	7.4	0.04	100	Mixed	0.34
Curve 3	3610	8.6	0.35	32	Mixed	4.22
Curve 4	3595	9.9	0.08	0	Mixed	1.17
Curve 5	3582	11.8	0.19	37	Mixed	3.17
Curve 6	3561	21.1	0.16	62	Mixed	4.26
Curve 7	3544	11.4	0.01	100	Mixed	0.18
Curve 8	3531	33.1	0.04	100	Mixed	1.38

FIGURE 11. IR single-crystal spectrum in the energy range of the OH^- stretching vibrations at RT of natural "end-member" andradite 4282 (Table 1) with fitted bands. (Color online.)

Water-poor intermediate composition grossular-andradite garnets. Many, if not most, Ca-rich silicate garnets in Earth's crust are grossular-andradite solid solutions that crystallize during metamorphism. There can be complete $Al \leftrightarrow Fe^{3+}$ exchange at [*Y*] across the join and the thermodynamic mixing behavior has been studied (Dachs and Geiger 2019). The cation mixing behavior can be complex because varying partial degrees in the long-range order can occur, decreasing the space group symmetry below cubic (Takéuchi et al. 1982). At any rate, water-poor grossular-andradite garnets offer an additional system for investigation, because their temperatures of crystallization are well above those where many water-rich crystals are stable. What do their IR spectra show?

Various IR spectra have been published (i.e., Rossman and Aines 1991; Phichaikamjornwut et al. 2012) and several garnets have been investigated in this work. Conceivably, it could be expected that spectral complexity could increase compared to the situation for end-member garnet species. The crystal chemistry of solid-solution garnets is more complex because of Al^{3+}-Fe^{3+} mixing at [*Y*]. Local OH^- vibrational behavior could be affected, as discussed above (Fig. 2). Assuming statistically random Al^{3+}-Fe^{3+} mixing, there can be five possible local *Y*-cation configurations around a single, common $(H_4O_4)^{4-}$ group. They are: Al-Al-Al-Al, Fe^{3+}-Al-Al-Al, Fe^{3+}-Fe^{3+}-Al-Al, Fe^{3+}-Fe^{3+}-Fe^{3+}-Al, and Fe^{3+}-Fe^{3+}-Fe^{3+}-Fe^{3+}. For the case of strict random mixing, the probability for each of the five configurations is a function of the bulk composition of the crystal. The situation becomes more complex, if additional $(H_4O_4)^{4-}$ groups are brought into the analysis. Suffice it to note that different energy OH^--stretching modes could potentially occur.

What is observed in the available IR spectra? To begin, many, water-poor $Ca_3(Al_x,Fe^{3+}_{1-x})_2Si_3O_{12}$ garnets show an OH^- mode at 3563 cm^{-1} at RT. Following the analysis for the case of "end-member" andradite, it can be assigned to a single, isolated $(H_4O_4)^{4-}$ group surrounded by Fe^{3+} cations. Clearly, the spectra of a number of Fe^{3+}-bearing grossulars in Rossman and Aines (1991) show the presence of an OH^- band at about 3563 cm^{-1} (their Figs. 4, 5, 6, 8, 9, and 10 and samples 1125, 936, 1042, 1051, 1430, 938, 1327, 1357, and 1411, for example). The same is true for the IR spectra of several grossular-andradite garnets in Phichaikamjornwut et al. (2012). In addition, OH^- modes at 3581 and 3594 cm^{-1} are also observed in the spectra of some of these grossular-andradite garnets with the assignments given above and in Table 2.

Take two specific examples, the first being garnet 6741 (Table 1) of approximate composition $Gro_{73}And_{23}$. Its IR spectrum was recorded at 273 and 80 K (Fig. 12a). At 273 K three distinct and relatively strong OH^- bands are observable (i.e., 3688, 3666, and 3629 cm^{-1}) and at 80 K four bands (i.e., 3694, 3672, 3634, and 3615 cm^{-1}). Weak bands (i.e., 3565 cm^{-1} at 273 K and 3562 cm^{-1} at 80 K) and shoulders can also be discerned. In the case of this garnet, it is important to bear in mind that, although

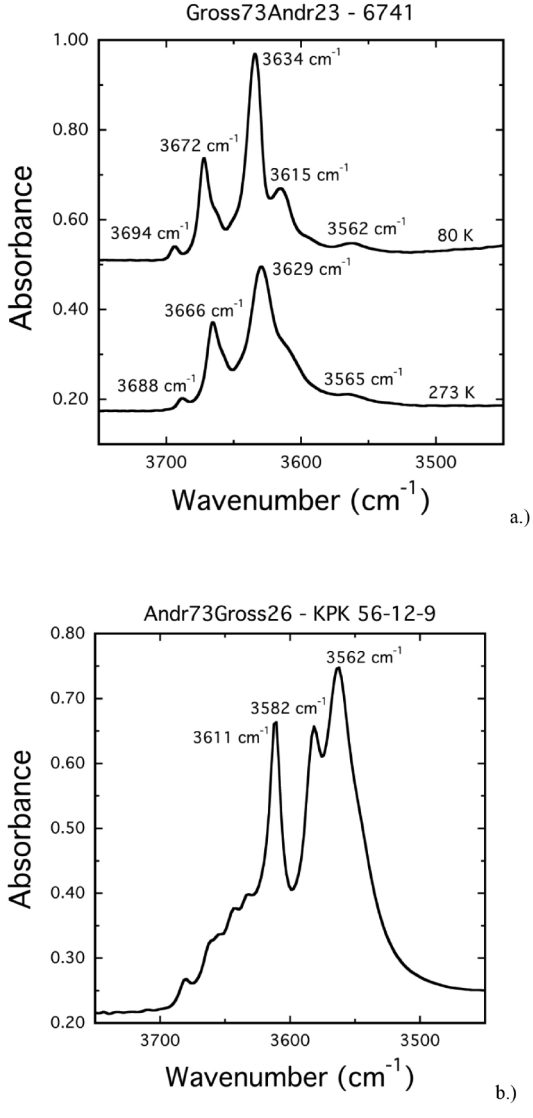

FIGURE 12. IR single-crystal spectra in the energy range of the OH^- stretching vibrations for: (**a**) sample 6741 of composition grossular73-andradite23 at 273 and 80 K and (**b**) sample KPK 56-12-9 of composition andradite73-grossular26 at RT. Sample description in Table 1.

it has a considerable 25 mol% andradite component, nearly all of the OH^- is contained in various hydrogrossular-like clusters. The simplest interpretation is that the energetics associated with the formation of hydrogrossular-like clusters are more favorable than for hydroandradite-like clusters. This proposal is consistent with synthesis experiment results (Flint et al. 1941; Dilnesa et al. 2014) for garnets in the system $Ca_3Al_2(SiO_4)_3$-$Ca_3Al_2(H_4O_4)_3$-$Ca_3Fe_2^{3+}(SiO_4)_3$-$Ca_3Fe_2^{3+}(H_4O_4)_3$ as shown in Figure 1. Only the binary $Ca_3Al_2(SiO_4)_3$-$Ca_3Al_2(H_4O_4)_3$ shows complete solid solution from end-member to end-member.

Finally, consider the RT spectrum of an andradite garnet of composition $And_{76}Gr_{23}$ (sample KPK 56-12-9 of Phichaikamjornwut et al. 2012) shown in Figure 12b. It shows three strong OH^- bands with the two lowest wavenumber ones occurring at 3562 and 3582 cm^{-1}. They are associated with hydroandradite-like clusters (Table 2). The mode at 3611 cm^{-1} is difficult to assign and could represent an end-member $Ca_3Fe_3^{2+}$-$H_{12}O_{12}$-like or a hydrogrossular-like cluster (Table 2). The various weak bands, observable at higher wavenumbers, probably represent hydrogrossular clusters present in small amounts. At any rate, the bulk of the OH^--like clusters in this solid-solution garnet is partitioned into hydroandradite-like clusters. Research needs to be done to determine the nature of H_2O partitioning and hydrogarnet-cluster formation in the nominally anhydrous system $Ca_3(Al_x,Fe_{1-x}^{3+})_2Si_3O_{12}$. In other words, the role of garnet composition with regards to the nature of structural "water" needs to be investigated as a function of P_{H_2O} and T.

IMPLICATIONS

Considerable and diverse research have been undertaken on various "water"-bearing garnets over the last approximate four decades. And, here, it should be noted that in terms of the many "end-member" grossular samples, which have been studied by IR spectroscopy, that we are not aware of any "water"-free crystals. This is an important observation. Much has been learned, but much is still not understood. What is presently the state of the field, and what needs to be done?

Previously, the IR and Raman spectra of different composition calcium silicate garnets could not be interpreted in any systematic and rational manner. Spectroscopic interpretation was often speculative with no rigorous scientific basis or it was simply not undertaken. It appears that proposals linking the large number of observed OH^- bands to different atomic mechanisms involving "defects" or "non-standard" garnet elements (see Geiger and Rossman 2020b, this issue) are probably not fully correct. That is, chemistry and various defects were taken as the deciding factor in the nature of OH^- incorporation in many garnets. The model analysis presented here, if correct, simplifies the nature of OH^--substitution, by returning back to the central importance of the well-known hydrogarnet substitution, namely $(H_4O_4)^{4-} \leftrightarrow (SiO_4)^{4-}$ or $4(H^+) \leftrightarrow (Si)^{4+}$. The varying and complex IR spectra of different calcium silicate garnets reflect the presence of various local microscopic- and nano-size $Ca_3Al_2H_{12}O_{12}$- and $Ca_3Fe_2^{3+}H_{12}O_{12}$-like clusters. Inclusion phases, probably hydrous layer silicates, can also give rise to OH^- bands. We want to emphasize that this is not to say that other OH^- substitutional mechanisms cannot occur in silicate garnet.

Open questions regarding spectroscopy remain. Intense OH^- bands at wavenumbers less than 3560 cm^{-1} are often observed in IR spectra of garnet. Further research is needed to interpret and assign them. It needs to be determined if there are different IR absorption coefficients associated with the different modes. A crystal-chemical question that arises, is how OH^- can be incorporated in certain, other nominally anhydrous silicates? Could proton clustering play a role in any of them as well? Several more mineralogical, petrological, and geochemical issues remain to be studied. Concluding, it goes without saying that research on garnet has entered a new phase. Further issues relating to "water" in Ca silicate garnets are discussed in Part II (Geiger and Rossman 2020b) of this investigation.

ACKNOWLEDGMENTS

B. Lothenbach kindly supplied the synthetic hydrogarnets and B. Phichaikamjornwut provided her IR data on grossular and andradite garnets for analysis. E. Grew assisted in constructing Figure 1. E. Libowitzky made constructive comments that improved the manuscript.

FUNDING

This research was supported by grants from the Austrian Science Fund (FWF: P 30977-NBL) to C.A.G. and NSF (EAR-1322082) to G.R.R. C.A.G. also thanks the "Land Salzburg" for financial support through the initiative "Wissenschafts- und Innovationsstrategie Salzburg 2025."

REFERENCES CITED

Adamo, I., Gatta, G.D., Rotiroti, N., Diella, V., and Pavese, A. (2011) Green andradite stones: gemmological and mineralogical characterisation. European Journal of Mineralogy, 23, 91–100.

Aines, R.D., and Rossman, G.R. (1984) The hydrous component in garnets: pyralspites. American Mineralogist, 69, 1116–1126.

Albrecht, R., Hunger, J., Doert, T., and Ruck, M. (2019) Syntheses, crystal structures and physical properties of chromium and rhodium hydrogarnets $Ca[Cr(OH)_6]_2$, $Sr[Cr(OH)_6]_2$, and $Sr[Rh(OH)_6]_2$. European Journal of Inorganic Chemistry, 10, 1398–1405.

Allen, F.M., and Busek, P.R. (1988) XRD, FTIR, and TEM studies of optically anisotropic grossular garnets. American Mineralogist, 73, 568–584.

Amthauer, G., and Rossman, G.R. (1998) The hydrous component in andradite garnet. American Mineralogist, 83, 835–840.

Armbruster, T. (1995) Structure refinement of hydrous andradite $Ca_3Fe_{1.54}Mn_{0.20}Al_{0.26}(SiO_4)_{1.65}(O_4H_4)_{1.35}$, from the Wessels mine, Kalahari manganese field, South Africa. European Journal of Mineralogy, 7, 1221–1225.

Armbruster, T., and Geiger, C.A. (1993) Andradite crystal chemistry, dynamic X-site disorder and strain in silicate garnets. European Journal of Mineralogy, 5, 59–71.

Basso, R., and Cabella, R. (1990) Crystal chemical study of garnets from metarodingites in the Voltri Group metaophiolites (Ligurian Alps, Italy). Neues Jahrbuch für Mineralogie Monatshefte, 3, 127–136.

Basso, R. Cimmino, F., and Messiga, B. (1984) Crystal chemistry of hydrogarnets from three different microstructural sites of a basaltic metarodingite from the Voltri Massif (Western Liguria, Italy). Neues Jahrbuch für Mineralogie Abhandlungen, 148, 246–258.

Bell, D.R., and Rossman, G.R. (1992) Water in Earth's mantle: The role of nominally anhydrous minerals. Science, 255, 1391–1397.

Belyankin, D.S., and Petrov, V.P. (1939) Hibschite in Georgia. Doklady of the Academy of Sciences, U.S.S.R, 24, 349–352.

——— (1941a) Reexamining the chemical formula of hibschite. Doklady of the Academy of Sciences, U.S.S.R, 30, 66–68.

——— (1941b) The grossularoid group (hibschite, plazolite). American Mineralogist, 26, 450–453.

Beran, A., Sturma, R. and Zemann, J. (1983) Ultrarotspektroskopische Untersuchungen über den OH-Gehalt einiger Granate. Österreichische Akademie der Wissenschaften, Mathmatisch-naturwissenschafte Klasse, 75–79.

Birkett, T.C., and Trzcienski, W.E. Jr. (1984) Hydrogarnet: Multi-site hydrogen occupancy in the garnet structure. Canadian Mineralogist, 22, 675–680.

Carlson, E.T. (1956) Hydrogarnet formation in the system lime-alumina-silica-water. Journal of Research of the National Bureau of Standards, 56, 327–335.

Cho, H., and Rossman, G.R. (1993) Single-crystal NMR studies of low-concentration hydrous species in minerals: Grossular garnet. American Mineralogist, 78, 1149–1164.

Cohen-Addad, C., Ducros, P., and Bertaut, E.F. (1967) Étude de la substitution du groupement SiO_4 par $(OH)_4$ dans les composés $Al_2Ca_3(OH)_{12}$ et $Al_2Ca_3(SiO_4)_{2.16}(OH)_{3.36}$ de type grenat. Acta Crystallographica, 23, 220–230.

Cornu, F. (1905) «Hibschit» aus Einschlüssen des oberturonen Kalkmergels der Cuvieristufe im Phonolit des Marienberges bei Aussig. Tschermaks mineralogische und petrographische Mitteilungen, 24, 327–328.

——— (1906) Hibschit, ein neues Kontaktmineral. Tschermaks mineralogische und petrographische Mitteilungen, 25, 249–268.

Dachs, E., and Geiger, C.A. (2019) Thermodynamic behaviour of grossular–andradite, $Ca_3(Al_xFe^{3+}_{1-x})_2Si_3O_{12}$, garnets: a calorimetric study. European Journal of Mineralogy, 31, 443–451.

Dachs, E., Geiger, C.A., Benisek, A., and Grevel, K-D. (2012) Grossular: A crystal-chemical, calorimetric, and thermodynamic study. American Mineralogist, 97, 1299–1313.

Dilnesa, B.Z., Lothenbach, B., Renaudin, G., Wichser, A., and Kulik, D. (2014) Synthesis and characrterization of $Ca_3(Al_xFe_{1-x})_2(SiO_4)_y(OH)_{4(3-y)}$. Cement and Concrete Research, 59, 96–111.

Ferro, O., Galli, E., Papp, G., Quartieri, S., Szakáll, S., and Vezzalini, G. (2003) A new occurrence of katoite and re-examination of the hydrogrossular group. European Journal of Mineralogy, 15, 419–426.

Flint, E.P., and Wells, L.S. (1941) Relationship of the garnet-hydrogarnet series to the sulfate resistance of portland cement. Journal of Research of the National Bureau of Standards, 27, Research Paper RP, 1411, 171–180.

Flint, E.P., McMurdie, H.F., and Wells, L.S. (1941) Hydrothermal and X-ray studies of the garnet-hydrogarnet series and the relationship of the series to hydration products of portland cement. National Bureau of Standards, Research, 26, Paper RP, 1335, 13–33.

Foreman, D.W. Jr. (1968) Neutron and X-ray diffraction study of $Ca_3Al_2(O_4D_4)_3$, a garnetoid. The Journal of Chemical Physics, 48, 3037–3041.

Foshag, W.F. (1920) Plazolite, a new mineral. American Mineralogist, 5, 183–185.

Geiger, C.A. (1998) A powder infrared spectroscopic investigation of garnet binaries in the system $Mg_3Al_2Si_3O_{12}$-$Fe_3Al_2Si_3O_{12}$-$Mn_3Al_2Si_3O_{12}$-$Ca_3Al_2Si_3O_{12}$. European Journal of Mineralogy, 3, 407–422.

——— (2008) Silicate garnet: A micro to macroscopic (re)view. American Mineralogist, 93, 360–372.

——— (2013) Garnet: A key phase in nature, the laboratory and in technology. Elements, 9, 447–452.

Geiger, C.A., and Armbruster, T. (1997) $Mn_3Al_2Si_3O_{12}$ spessartine and $Ca_3Al_2Si_3O_{12}$ grossular garnet: dynamical structural and thermodynamic properties. American Mineralogist, 82, 740–747.

Geiger, C.A., and Rossman, G.R. (2018) IR spectroscopy and OH^- in silicate garnet: The long quest to document the hydrogarnet substitution. American Mineralogist, 103, 384–393.

Geiger, C.A. and Rossman, G.R. (2020b) Micro- and nano-size hydrogarnet clusters in calcium silicate garnet: Part II. Mineralogical, petrological, and geochemical aspects. American Mineralogist, 105, 468–478.

Geiger, C.A., Dachs, E., Vielreicher, N., and Rossman, G.R. (2018) Heat capacity and entropy behavior of andradite: A multi-sample and -methodological investigation. European Journal of Mineralogy, 30, 681–694.

Grew, E.S., Locock, A.J., Mills, S.J., Galuskina, I.O., Galuskin, E.V., and Hålenius, U. (2013) Nomenclature of the garnet supergroup. American Mineralogist, 98, 785–811.

Harmon, K.M., Gabriele, J.M., and Nuttall, A.S. (1982) Hydrogen bonding in the tetrahedral $O_4H_4^{4-}$-cluster in hydrogrossular. Journal of Molecular Structure, 82, 213–219.

Heller-Kallai, L., Yariv, S., and Gross, S. (1975) Hydroxyl-stretching frequencies of serpentine minerals. Mineralogical Magazine, 40, 197–200.

Hofmeister, A.M., and Chopelas, A. (1991) Vibrational spectroscopy of end-member silicate garnets. Physics and Chemistry of Minerals, 17, 503–526.

Hsu, L.C. (1980) Hydration and phase relations of grossular-spessartine garnets at P_{H_2O} = 2 Kb. Contributions to Mineralogy and Petrology, 71, 407–415.

Ingrin, J., and Skogby, H. (2000) Hydrogen in nominally anhydrous upper-mantle minerals: concentration levels and implications. European Journal of Mineralogy, 12, 543–570.

Ito, J., and Frondel, C. (1967) New synthetic hydrogarnets. American Mineralogist, 52, 1105–1109.

Jappy, T.G., and Glasser, F.P. (1991) Synthesis and stability of silica-substituted hydrogarnet $Ca_3Al_2Si_{3-x}O_{12-4x}(OH)_{4x}$. Advances in Cement Research, 4, 1–8.

Kobayashi, S., and Shoji, T. (1983) Infrared analysis of the grossular-hydrogrossular series. Mineralogical Journal, 11, 331–343.

Kolesov, B.A., and Geiger, C.A. (1998) Raman spectra of silicate garnets. Physics and Chemistry of Minerals, 25, 142–151.

——— (2005) The vibrational spectrum of synthetic hydrogrossular (katoite) $Ca_3Al_2(O_4H_4)_3$: A low temperature IR and Raman spectroscopic study. American Mineralogist, 90, 1335–1341.

Kresten, P., Nairis, H.J., and Wadsten, T. (1982) Hydroandradite from Alnö Island, Sweden. Geologiska Föreningens i Stockholm Förhandlingar, 104, 240.

Kurka, A., Blanchard, M., and Ingrin, J. (2005) Kinetics of hydrogen extraction and deuteration in grossular. Mineralogical Magazine, 69, 359–371.

Kuzel, H.-J. (1968) Über die Diadochie von Al^{3+}, Cr^{3+}, und Fe^{3+} in $3CaO{\cdot}Al_2O_3{\cdot}6H_2O$ oberhalb 50 °C. Neues Jahrbuch für Mineralogie Monatshefte, 87–96.

Lager, G.A., and von Dreele, R.B. (1996) Neutron powder diffraction study of hydrogarnet to 9.0 GPa. American Mineralogist, 81, 1097–1104.

Lager, G.A., Armbruster, T., and Faber, G. (1987) Neutron and X-ray diffraction study of hydrogarnet $Ca_3Al_2(O_4H_4)_3$. American Mineralogist, 72, 756–765.

Lager, G.A., Downs, R.T., Origlieri, M., and Garoutte, R. (2002) High-pressure single-crystal X-ray study of katoite hydrogarnet: Evidence for a phase transition from *Ia3d* → *I43d* symmetry at 5 GPa. American Mineralogist, 87, 642–647.

Li, G., Feng, S., Li, L., Li, X., and Jin, W. (1997) Mild hydrothermal syntheses and thermal behaviors of hydrogarnets $Sr_3M_2(OH)_{12}$ (M = Cr, Fe, and Al). Chemistry of Materials, 9, 2894–2901.

Maldener, J., Hösch, A., Langer, K., and Rauch, F. (2003) Hydrogen in some natural garnets studied by nuclear reaction analysis and vibrational spectroscopy. Physics and Chemistry of Minerals, 30, 337–344.

McAloon, B.P., and Hofmeister, A.M. (1993) Single-crystal absorption and reflection infrared spectroscopy of birefringent grossular-andradite garnets. American Mineralogist, 78, 957–967.

Mellini, M., Fuchs, Y., Viti, C., Lemaire, C., and Linarès, J. (2002) Insights into the antigorite structure from Mössbauer and FTIR spectroscopies. European Journal of Mineralogy, 14, 97–104.

Moore, R.K., White, W.B., and Long, T. (1971) Vibrational spectra of the common silicates: I. The garnets. American Mineralogist, 56, 54–71.

Nakamoto, K. (2009) Infrared and Raman Spectra of Inorganic and Coordination Compounds, Part A: Theory and Applications in Inorganic Chemistry, 6th ed., 419 p. Wiley.

Nevsky, N.N., Ivanov-Emin, B.N., Nevskaya, N.A., Kaziev, G.Z., and Belov, N.V. (1982) Crystal structure of strontium garnets. Doklady Akademii Nauk SSSR, 264, 857–858 (in Russian).

Novak, G.A., and Gibbs, G.V. (1971) The crystal chemistry of the silicate garnets. American Mineralogist, 56, 791–825.

Orlando, R., Torres, F.J., Pascale, F., Ugliengo, P., Zicocvich-Wilson, C., and Dovesi, R. (2006) Vibrational spectrum of katoite $Ca_3Al_2[(OH)_4]_3$: A periodic ab initio study. Journal of Physical Chemistry B, 110, 692–701.

Pabst, A. (1942) Reexamination of hibschite. American Mineralogist, 27, 783–792.

Palke, A.C., Stebbins, J.F., Geiger, C.A., and Tippelt, G. (2015) Cation order-disorder in Fe-bearing pyrope and grossular garnets: An ^{27}Al and ^{29}Si MAS NMR and ^{57}Fe Mössbauer spectroscopy study. American Mineralogist, 100, 536–547.

Passaglia, E., and Rinaldi, R. (1984) Katoite, a new member of the $Ca_3Al_2(SiO_4)_3$-$Ca_3Al_2(OH)_{12}$ series and a new nomenclature for the hydrogrossular group of minerals. Bulletin de Minéralogie, 107, 605–618.

Peslier, A.H. (2010) A review of water contents of nominally anhydrous natural minerals in the mantles of Earth, Mars and the Moon. Journal of Volcanology and Geothermal Research, 197, 239–258.

Phichaikamjornwut, B., Skogby, H., Ounchanum, P., Limtrakun, P., and Boonsoong, A. (2012) Hydrous components of grossular-andradite garnets from Thailand: thermal stability and exchange kinetics. European Journal of Mineralogy, 24, 107–121.

Pistorius, C.W.F.T., and Kennedy, G.C. (1960) Stability relations of grossularite and hydrogrossularite at high temperatures and pressures. American Journal of Science, 258, 247–257.

Reynes, J., Jollands, M., Hermann, J., and Ireland (2018) Experimental constraints on hydrogen diffusion in garnet. Contributions to Mineralogy and Petrology, 173, 23.

Rossman, G.R., and Aines, R.D. (1986) Spectroscopy of a birefringent grossular from Asbestos, Quebec, Canada. American Mineralogist, 71, 779–780.

——— (1991) The hydrous components in garnets: Grossular-hydrogrossular. American Mineralogist, 76, 1153–1164.

Schroeder, P.A. (2002) Infrared Spectroscopy in clay science. In A. Rule and S. Guggenheim, Eds., Teaching Clay Science, 11, p. 181–206. CMS Workshop Lectures, The Clay Mineral Society.

Takéuchi, Y., Haga, N., Umizu, S., and Sato, G. (1982) The derivative structure of silicate garnets in grandite. Zeitschrift für Kristallographie, 158, 53–99.

Thorvaldson, T., and Grace, N.S. (1929) The hydration of the aluminates of calcium. I. A new crystalline form of hydrated tricalcium aluminate. Canadian Journal of Research, 1, 36–47.

Thorvaldson, T., Grace, N.S., and Vigfusson, V.A. (1929) The hydration of the aluminates of calcium. II. The hydration products of tricalcium aluminate. Canadian Journal of Research, 1, 201–213.

Wilkins, R.W.T., and Sabine, W. (1973) Water content of some nominally anhydrous silicates. American Mineralogist, 58, 508–516.

Withers, A.C., Wood, B.J., and Carroll, M.R. (1998) The OH content of pyrope at high pressure. Chemical Geology, 147, 161–171.

Woodford, A.O., Crippen, R.A., and Garner, K.B. (1941) Section across Commercial quarry, Crestmore, California. American Mineralogist, 26, 351–381.

Wright, K., Freer, R., and Catlow, C.R.A. (1994) The energetics and structure of the hydrogarnet defect in grossular: A computer simulation study. Physics and Chemistry of Minerals, 20, 500–503.

Yoder, H.S. Jr. (1950) Stability relations of grossularite. The Journal of Geology, 58, 221–253.

Zhang, P., Ingrin, J., Depecker, C., and Xia, Q. (2015) Kinetics of deuteration in andradite and garnet. American Mineralogist, 100, 1400–1410.

Manuscript received August 12, 2019
Manuscript accepted November 20, 2019
Manuscript handled by Roland Stalder